

RSC Advances



This is an *Accepted Manuscript*, which has been through the Royal Society of Chemistry peer review process and has been accepted for publication.

Accepted Manuscripts are published online shortly after acceptance, before technical editing, formatting and proof reading. Using this free service, authors can make their results available to the community, in citable form, before we publish the edited article. This *Accepted Manuscript* will be replaced by the edited, formatted and paginated article as soon as this is available.

You can find more information about *Accepted Manuscripts* in the [Information for Authors](#).

Please note that technical editing may introduce minor changes to the text and/or graphics, which may alter content. The journal's standard [Terms & Conditions](#) and the [Ethical guidelines](#) still apply. In no event shall the Royal Society of Chemistry be held responsible for any errors or omissions in this *Accepted Manuscript* or any consequences arising from the use of any information it contains.

Fabrication of Spinel Ferrite based Alkaline Anion Exchange Membrane Water Electrolysers for Hydrogen Production

T.Pandiarajan and S.Ravichandran*

**Electro Inorganic Chemicals Division,
CSIR-Central Electrochemical Research Institute, Karaikudi-630006
India**

Corresponding Author:

Srravi371@gmail.com

Abstract

Alkaline anion exchange membrane water electrolysis (AEMWE) is considered to be an alternative to proton exchange membrane water electrolysis (PEMWE), owing to the use of non-noble meta/metal oxides in AEMWE. Here, we report a highly durable and low-cost AEM-based electrolysis cell with, active spinel ferrite catalysts for hydrogen production. Ce-substituted MnFe_2O_4 was synthesized by a combustion method and investigated as electro catalysts for oxygen evolution reactions (OERs). Substitution of Ce in the cubic lattice of MnFe_2O_4 increases the conductivity of $\text{Ce}_x\text{MnFe}_{(2-x)}\text{O}_4$, which results in a negative shift in the OER onset potential. At 25°C, single cell with $\text{Ce}_{0.2}\text{MnFe}_{1.8}\text{O}_4$ exhibited a current density of $300\text{mA}/\text{cm}^2$ at 1.8V with deionized water. Notably, $\text{Ce}_{0.2}\text{MnFe}_{1.8}\text{O}_4$ demonstrates a durability of >100 hours on constant electrolysis.

Key words: Alkaline anion exchange membrane, alkaline Water electrolysis, single cell, Hydrogen production, Ce-doped MnFe_2O_4

1. Introduction

The gradual march of the world toward a serious energy crisis has motivated passionate studies on alternative energy conversion and storage systems¹⁻⁵. To determine the ultimate renewable energy source for the future, a number of energy conversion and storage techniques have been developed, such as water splitting, fuel cells, and batteries, etc⁶⁻⁸. One of the most promising energy conversion methods, electrochemical water splitting, has received much attention due to its commercial efficiency and minimal impact on the environment^{3,9,10}. Alkaline water electrolysis (AWE) is the simplest and cheaper method for producing hydrogen, and is recognized as an efficient fuel for energy storage systems. Moreover, AWE has dominated large-scale hydrogen production technology for several decades, because of cost-effective electrolyser fabrication and the simple control of corrosion¹¹⁻¹⁵. However, conventional liquid alkaline electrolysers face a set of challenges, such as limited current density, low operating pressure, and low partial load range.^{11,16} These challenges are due to the use of an electrolyte composed of 10–30% KOH solution in liquid alkaline water electrolysers for the electro catalytic water splitting.

The problems associated with the use of a concentrated alkali are largely related to the formation of carbonate ions, which can decrease the electrolyser lifetime and purity of hydrogen¹⁷⁻¹⁹. As a result, water electrolysis via solid polymer electrolyte (SPE), viz. proton exchange membranes (PEMs), and anion exchange membranes (AEMs) have recently received greater attention. Moreover, an alkaline polymer electrolyte possesses the advantages of both a solid polymer electrolyte and an alkaline pH.

While PEM water electrolysis (PEMWE) offers high current densities, compact electrolyser designs, and high hydrogen production rates, the non-platinum group metal lacks durability in an acidic environment^{9,16}. Furthermore, the fabrication of the membrane electrode assembly (MEA) for PEMWE is expensive, resulting in resources being diverted to the development of alkaline anion exchange membrane water electrolysis (AEMWE)^{20,21}.

The efficiency of electrolysers depends on the MEA, a key component of water electrolysis that hinges on the sluggish kinetic reactions of oxygen evolution (OER) and oxygen reduction reaction (ORR). Although the OER activity of noble metal oxides (Ir, Ru, and Pt) was outstanding in acidic medium, stability problems under alkaline conditions prevent the utilization of noble metal oxides as a practical electro catalyst for OER²²⁻²⁴.

The exhaustive search for non-noble catalysts, conducted over many years, has identified the mixed metal oxides,^{25,26} specifically the AB_2O_4 spinel,²⁷⁻³¹ spinel ferrites,³²⁻³⁴ organic compounds,³⁵ and perovskites,^{6,36-38} as potential OER catalysts capable of replacing expensive noble metal-based compounds. A detailed discussion of the electrocatalytic activities of non-noble metal oxides can be found in the cited reference [37]. Moreover, several studies have reported Ni and Co-based materials as excellent catalysts for water oxidation,³⁷ but only in alkaline solution; changing the electrolyte to deionized water significantly decreases the efficiency of electrolysers. To date, only a few studies have addressed AAEMWE in deionized water. For example, Xu Wu et al have reported a current density of $100\text{mA}/\text{cm}^2$ at 1.8V (25°C) for MEA with $\text{Cu}_{0.7}\text{Co}_{2.3}\text{O}_4$ ³⁹. In addition, a current density of $300\text{ mA}/\text{cm}^2$ at 2.2-2.5V with a $\text{Li}_{0.21}\text{Co}_{2.79}\text{O}_4$ anode has been reported⁴⁰. More recently, Lin Zhuang and co-workers⁴¹ demonstrated a current density of $400\text{ mA}/\text{cm}^2$ at 1.85V with a Ni-Mo-based AEM electrolyser

using only deionized water. Similarly, Chao-yang Wang et al.¹⁸ report a life-time of >500 h with AEM water electrolysis. However, the Ni-Mo-based AEM electrolyser exhibits a durability of only 8 h, and the latter requires noble metal oxides for long-term stability. Moreover, each of these electrolysers required an operating temperature of 50 to 75°C.

Therefore, the challenge of developing a non-noble metal catalysts for AEMWE that exhibits a current density of $j > 0.5 \text{ A cm}^{-2}$ at an over potential of $\eta_{\text{O}_2} < 0.3 \text{ V}$ with long-term stability, at room temperature remains to be achieved.

Among non-noble metal catalysts, spinel ferrites³² are of particular interest because they possess low-cost, high catalytic activity, and durability at high pH; such attributes make spinel ferrites relevant for use in catalysis, sensors, and magnetic devices. Moreover, the spinel ferrite based catalysts demonstrate a great potential for OER^{33,34,42-44} and ORR,⁴⁵ which is comparable to commercial Pt. However, in practice, the low electrical conductivity restricts the application of spinel ferrite as a catalyst. Here, we report the performance of a laboratory scale AAEMWE with spinel ferrite catalysts for pure hydrogen production.

2. Experimental section

2.1. Membrane Pre-treatment

The Alkaline Anion Exchange Membrane (Fumasep[®] FAA-3-PK-130) was purchased from the Fumatech company (Germany), delivered in bromide form and dry state. The membrane thickness was 130 μm and the specific conductivity was 7.6 mS cm^{-1} at 25°C. For alkaline applications, the membrane must be converted into a hydroxyl form. To achieve this, the membrane was kept in an aqueous solution of 1 M KOH for 24 h at 20-30°C, and then

transferred to deionized water for 1 h. To avoid CO₂ contamination, the pre-treated membrane was stored under humidified and CO₂ free conditions.

2.2. Ionomer Preparation

Instead of using commercial ionomer solution, we used the AAEM dissolved in dimethyl sulfoxide (DMSO) solvent. To prepare AAEM ionomer solution 0.1g of AAEM was added to 3ml of DMSO solvent. However, the substrate used as a support for membrane not dissolved completely in the DMSO and settle down as precipitate. So we discard the precipitate and used the solution as ionomer for catalyst ink preparation.

2.3 Catalyst ink preparation

To prepare the catalyst ink, 3.5mg of the catalyst powder dispersed, in the mixture of 60 μ ml AAEM solution, 2 ml of 2-propanol and 30 μ ml deionized water. After 30 minutes of sonication, the solution became homogeneous and was used for the MEA preparation.

2.4. MEA preparation:

The MEA was fabricated by brush coating the catalyst mixture onto each side of the membrane, which was allowed to dry and hot pressed at 70°C. The catalyst loadings on the anode and cathode were 3.5 mg/cm² of Ce_{0.2}MnFe_{1.8}O₄ and Ni powder (sigma Aldrich) respectively. This was followed by the cell assembly, utilizing a pair of platinum-coated titanium mesh as current collectors. The current collectors were placed on each side of the MEA to ensure proper contact between electrodes and the current carrier plate. Finally, a stainless steel end plate was placed for mechanical support. Fig.7 shows the schematic diagram of the single cell adopted for this work. The working area of the single cell was

2cm*2cm. The single-cell experiments were carried out using deionized water. Polarisation curves of the single cell with $Ce_xMnFe_{2-x}O_4$ were measured with a scan rate of 1mV/s.

3.0 Results & discussions

3.1. Half-Cell studies:

In our previous work,⁴⁶ we performed the initial screening of catalysts in a standard three-electrode system using various concentrations of KOH electrolytes and showed that 0.2M cerium substitution enhances the electrocatalytic activity of $MnFe_2O_4$ for OER in alkaline solution.

The Working electrode for electrochemical studies was prepared by sonicating 3mg of the catalyst, in 60 μ l isopropyl alcohol for 15minutes.20 μ l of the suspension was pipette out and dried on a pt metal substrate (1cm \times 1cm) by heating, in a pre-heated oven at 80°C. Subsequently the substrate was sintered, at 1200°C in presence of air for 2 h.

The X-ray diffractograms of the as prepared $MnFe_2O_4$ and $Ce_{0.2}Fe_{1.8}O_4$ are shown in **Fig.1**.The reflection patterns are distinct and sharp, clearly delineating the crystalline nature of the $Ce_xFe_{2-x}O_4$. Furthermore, the observed diffraction patterns of $MnFe_2O_4$ are good agreement with the spinel- type $MnFe_2O_4$ (**JCPDS: 073-1964**), with a cubic lattice spinel structure. Due to the large ionic radius the incorporation of Ce^{3+} in the spinel lattice increases the lattice constant value of $MnFe_2O_4$ ⁴⁷ from $a=8.515 \text{ \AA}$ to 8.614 \AA . The substitution of Ce^{3+} on $MnFe_2O_4$ was confirmed by X-ray photoelectron spectroscopy (XPS).

Fig. 2 illustrates the XPS spectrum of the $\text{Ce}_{0.2}\text{Fe}_{1.8}\text{O}_4$ after sintering at 1200°C , in ambient air for 2 hours. The survey spectrum presented in **Fig.2A**, shows the compositional elements of the $\text{Ce}_{0.2}\text{Fe}_{1.8}\text{O}_4$. Moreover, the elemental composition of Ce^{3+} , Mn^{2+} , and Fe^{3+} were further analyzed with the EDAX spectrum (**Fig.2B**).

Fig. 3A shows the XPS spectra for Mn 2p which provides clear evidence for the presence of Mn^{2+} in the $\text{Ce}_x\text{MnFe}_{2-x}\text{O}_4$. It can be seen from the spectrum that the peaks at 641.5 and 652.3 eV are caused by Mn 2p_{3/2} and Mn 2p_{1/2} respectively, with a satellite peak at 41.3eV^{43, 48}. In **Fig. 3C**, the peaks at 711.0 and 724.6 eV were respectively assigned to Fe 2p_{3/2} and Fe 2p_{1/2}⁴³. Moreover, two main peaks at 718.5 and 732.5 eV⁴⁹⁻⁵¹ specifies the presence of Fe^{3+} . Similarly, the characterized peaks with binding energies 845 and 905 eV⁵²⁻⁵⁴ in the XPS spectra (**Fig.3B**) occurs due to the presence of Ce^{3+} on MnFe_2O_4 . Thus, the above results clearly suggest that Ce^{3+} incorporated on MnFe_2O_4 and sintering the catalysts at 1200°C , resulted in the reduction of Fe^{3+} on the ferrite system.

As shown in **Fig.4**, the structural features of the prepared $\text{Ce}_x\text{Fe}_{2-x}\text{O}_4$ ($x=0.0, 0.2$) were analyzed using a scanning electron microscope (SEM). In all cases, we observed the collapsed microstructures of ferrites due to the high-temperature treatment. Further, sintering the samples at 1200°C increased the agglomeration of ferrites; this resulted in the formation of a thin-film layer³⁴. Subsequently, it insulates the Pt surface from the electrolyte solution. Therefore, no redox peaks appeared for Pt on cyclic Voltammetry studies of samples in KOH solution, which ruled out the synergetic effect or diffusion of Pt on the catalysts layers⁴². **Fig. 4C &4D** shows SEM recorded on samples coated on Pt surface and sintered in air for 2 hours at 1200°C .

The Cyclic voltammograms (CV) of catalysts were recorded in 1M KOH solution with a scan rate of 10mV/s at 25°C. **Fig.5** shows the CV curves recorded between 1.2-1.8V vs RHE). No redox peaks were seen in the CV⁴², indicating that the ferrite does not undergo any oxidation process in reaction conditions. However, the OER onset of Ce-substituted manganese ferrite shifts towards more negative than the pure compound.

A decrease in oxygen evolution overpotential (η_{O_2}) is observed by analyzing the electrochemical impedance spectrum (EIS) of the catalysts recorded during the OER (**Fig. 6**). The Ce-substituted $MnFe_2O_4$ shows smaller charge transfer resistance, compared to $MnFe_2O_4$. Such a drastic change in electrochemical behavior is due to the increase in the electronic conductivity of $Ce_{0.2}MnFe_{1.8}O_4$.

In general, the electrical conductivity of ferrites is explained by Verwey-de Boer mechanism and the polaron effect. However, the electrical conduction in ferrites originates between Fe^{2+} and Fe^{3+} ions at site B, conduction is mostly influenced by the Fe^{2+} concentration in the ferrite system. Due to the high temperature sintering, some lattice oxygen escapes from the spinel lattice, causing an oxygen deficiency in the spinel ferrites. Therefore, to balance the electrical charge created in the lattice unit, Fe^{3+} is reduced to Fe^{2+} .^{55,56}, which facilitates the formation of excess Fe^{2+} ions in the system (as shown in **Fig .3D**). Hence, the hopping rate of electrons in ferrites increases which is the cause of their higher electronic conductivity.^{55,57}

The X-ray photoelectron spectroscopy (XPS) spectrum, shown in figure 3C & 3D, confirms the co-existence of Fe^{2+} ions with Fe^{3+} in the spinel lattice. In addition, the replacement of metal ions with rare earth metal ions forms grain boundaries in ferrites; but using high concentration (≥ 0.4) of such metal ions lead to the formation of secondary phases (i.e. ABO_3) on the ferrite system. These secondary phases hinder the mobility of charge carriers and increase the electrical

resistivity. However, in the case of $\text{Ce}_{0.2}\text{MnFe}_{1.8}\text{O}_4$, the electronic conductivity was further enhanced by the cooperative effect⁵⁸ between the Ce^{3+} and Mn^{2+} . The interaction between the electron-rich Mn^{2+} and electron –deficient Ce^{3+} ion enhances the Lewis acid properties of the mixed valence centers, as a result, the electro catalytic activity of $\text{Ce}_{0.2}\text{MnFe}_{1.8}\text{O}_4$ increases.

3.2. Single Cell studies:

Based on results of half-cell studies, we selected $\text{Ce}_{0.2}\text{MnFe}_{1.8}\text{O}_4$ as a catalyst for single-cell experiments, since $\text{Ce}_{0.2}\text{MnFe}_{1.8}\text{O}_4$ demonstrates an excellent electro-catalytic activity and stability for OER, in alkaline solutions.

In general, the addition of the ionomer (during catalyst ink preparation) to the catalyst layer shows a direct effect on the efficiency of the electrolyser.^{59,60} This is because the ionomer addition promotes ion (H^+ or OH^-) transport from the bulk of the catalyst layer to the membrane, which consequently enhances the electrolyser efficiency by reducing the interfacial resistance between the membrane and electrode, or the ionomer and catalyst. Conversely, the electrical conductivity of catalysts is decreased by the addition of electron resistant ionomer solutions. Hence, it is important to optimize the ionomer loading for the catalyst ink and MEA preparation.

Furthermore, we modified the current collectors (Ti or stainless grids) by platinum-coating the Ti meshes for single cell studies. As commercial AEMs possess a lower conductivity than Nafion membranes, single cells based on AEMs are essentially sensitive to the requirement of a good current collector; which should be corrosion resistant, have strong electrical conductivity, and provide mechanical support to the membrane.^{16,61} Such a current collector should effectively expel the gases and allow the water to reach the catalytic sites in its counter flow. Hence, Pt-

coated Ti meshes are better choice, as they display good electrical properties and do not passivate over time. As a result, the performance and durability of the MEA may increase in electrochemical studies.

The electro catalytic performances of single cell with $\text{Ce}_{0.2}\text{MnFe}_{1.8}\text{O}_4$ and MnFe_2O_4 anodes were first evaluated by recording a Linear Sweep Voltammograms (LSV) in deionized water at room temperature. **Fig.8** shows the LSV curves of the MEA with $\text{Ce}_{0.2}\text{MnFe}_{1.8}\text{O}_4$ and MnFe_2O_4 anodes. At 25°C, the $\text{Ce}_{0.2}\text{MnFe}_{1.8}\text{O}_4$ exhibits an over potential of 320 mV for achieving a current density of $10\text{mA}/\text{cm}^2$, 80 mV lower than obtained on the MEA using MnFe_2O_4 in deionised water. When the $\text{Ce}_{0.2}\text{MnFe}_{1.8}\text{O}_4$ initiates the water splitting at 1.48V, the electrolyser starts with a current density of 3mA. Moreover, gradual increase the applied potential increases the current density to a maximum of $300\text{mA}/\text{cm}^2$ at 1.8V. The major change in the resistance values of MEA describes the high current density, beyond the potential of 1.55V. As shown in **Fig.9**, the potential above 1.55V the charge transfer values of MEA using $\text{Ce}_{0.2}\text{MnFe}_{1.8}\text{O}_4$ shifts significantly to smaller values and it accelerates the water splitting to a greater extent. To validate the synergistic effect or catalytic effect of Pt coated Ti meshes, we measured the polarization curve without catalysts on AAEM (**Fig. 8**). However, the single cell did not show any significant catalytic activity on water electrolysis, which ruled out the synergistic effect of Pt.

In contrast, the PEMWES using noble metal oxides will probably yield a maximum current density of $>1\text{A}/\text{cm}^2$ under similar voltage, due to the high conductivity of per fluorinated membranes (Nafion). However, our results are Superior to the electrolyzers with Co-based catalysts such as $\text{Cu}_{0.7}\text{Co}_{2.3}\text{O}_4$ ³⁹ and $\text{Li}_{0.21}\text{Co}_{2.79}\text{O}_4$ ⁴⁰ anodes. Though, the MEA with the above catalysts exhibit promising activity in KOH solution, they show only a small current density

performance in deionised water. Most significantly, the electro catalytic activity of $\text{Ce}_{0.2}\text{MnFe}_{1.8}\text{O}_4$ was comparable to the AAE water electrolyzers using Ni-Fe as the anode⁴¹. Previously, Hickner and Wang reported a maximum current density of $399\text{mA}/\text{cm}^2$ at 1.8V (50°C) with IrO₂ anode and Pt cathode. However, recently, Zhuang demonstrated the same current density with a slightly higher over potential and operating temperature of 75°C in AAEMWE using Ni-Fe anode working only with pure water. Although our experiments were carried out at room temperature, we achieved a performance comparable to that of the Ni-Fe anode performance at higher temperature. The electrocatalytic activities of various electrodes in deionized water are given in **Table 1**.

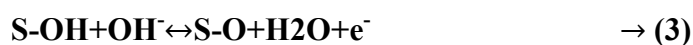
The efficiency of MEA depends on the effective utilization of catalysts for electrochemical reactions viz., OER and HER, which are ultimately governed by the quantity of intermediates that reach the catalyst surface. Here, we used an AEM ionomer solution prepared by dissolving pre-treated membrane in DMSO. As a result, it enhanced the hydroxyl ions transportation from the bulk catalyst layer to the membrane, and *vice versa*. Hence, the ionic conduction in the catalyst layer is significantly enhanced due to AAEM ionomer, and improves the electrolyser efficiency. Similarly, the Pt coated Ti meshes improve the durability of the electrolyzers by reducing the corrosion of anode components.^{61,40} Together with the ionomer effect and current collectors, the reduction of Fe^{3+} at high temperature also contributes for the overall efficiency of the single cell.

To evaluate the kinetic parameters (**Table.2**), we fit the polarization curves achieved with $\text{Ce}_{0.2}\text{MnFe}_{1.8}\text{O}_4$ and MnFe_2O_4 to the following equation.

$$\eta = a + b \log j \rightarrow \quad (1)$$

Where η is the over potential and j is the current density.

Fig.10 depicts the Tafel slope plots of MEA with $Ce_xMnFe_{2-x}O_4$ for OER measured in deionized water. The Tafel slope of $Ce_{0.2}MnFe_{1.8}O_4$ is 64mV/decade, lower than 45mV /decade obtained on the MEA using $MnFe_2O_4$. The observation of lower Tafel slope value for $Ce_{0.2}MnFe_{1.8}O_4$ compared to that of $MnFe_2O_4$ indicates the increased electron transfer for OER. A common mechanism for OER listed in equation (2), (3), and (4) has been used to account for the observed the kinetic parameters.



Where “S” is an active species

The Tafel slope (b) value of $Ce_{0.2}MnFe_{1.8}O_4$ indicates that the equation (3) is the rate determining step for OER. The literature studies^{39,42} show that if equation (3) is the rate determining step then it gives a second order reaction in OH^- and a typical b value of 60mV/decade. Again, it can be noticed from the discussions that, $Ce_{0.2}MnFe_{1.8}O_4$ was the most active catalyst for the OER among all $Ce_xMnFe_{2-x}O_4$.

Stability studies

The short term stability of the MEA estimated under an electrolysis current of 200mA/cm² at room temperature. During this study the cell voltage steadily increased with time (**Fig.11**). However, the commercial utilization of any catalyst requires long-term stability toward OER. As shown in **Fig. 12**, the stability of the $Ce_{0.2}MnFe_{1.8}O_4$ and $MnFe_2O_4$ was investigated by running chronoamperometric responses at 2V (vs. RHE) in deionized water. Current density

of $>390\text{mA}/\text{cm}^2$ remained constant. There was no apparent drop in the performance of $\text{Ce}_{0.2}\text{MnFe}_{1.8}\text{O}_4$ electrodes after 100 hrs. of operation. Moreover, we analyzed the electrolyte every 10 hrs. to ensure the stability of the catalysts during continuous electrolysis. Atomic absorption spectroscopy (AAS) analysis revealed negative results for the presence of metal ions, further supporting that these catalysts are stable during AEM water electrolysis.

4.0. Conclusion:

In summary, we concluded that the enhanced electrocatalytic activity of $\text{Ce}_{0.2}\text{MnFe}_{1.8}\text{O}_4$ results from the incorporation of Ce^{3+} into the MnFe_2O_4 spinel lattice. The single cell fabricated with $\text{Ce}_{0.2}\text{MnFe}_{1.8}\text{O}_4$ catalysts exhibit a current density of $\sim 300\text{mA}/\text{cm}^2$ at 1.8V in deionised water with a lifetime of >100 hrs on constant electrolysis. Moreover, our studies reveal that using Spinel ferrite as a catalyst; we can fabricate cost-effective, highly active AEM- based electrolyzers for water oxidation. Moreover, studies are on-going to investigate the temperature effect on water electrolysis and works to improve the efficiency of the cell.

Acknowledgements

T. Pandiarajan thanks UGC, India for providing Junior Research Fellowship. We also thank Mr A. Ram Kumar and M.Baskar, CSIR-CECRI, Karaikudi – for helping with the fabrication of single cell.

References

1. C. A. Rodriguez, M. A. Modestino, D. Psaltis and C. Moser, *Energy & Environmental Science*, 2014, 7, 3828-3835.
2. N. S. Lewis and D. G. Nocera, *Proceedings of the National Academy of Sciences*, 2006, 103, 15729-15735.
3. D. L. Stojić, M. P. Marčeta, S. P. Sovilj and Š. S. Miljanić, *Journal of Power Sources*, 2003, 118, 315-319.
4. H. B. Gray, *Nat Chem*, 2009, 1, 7-7.
5. M. G. Walter, E. L. Warren, J. R. McKone, S. W. Boettcher, Q. Mi, E. A. Santori and N. S. Lewis, *Chemical Reviews*, 2010, 110, 6446-6473.
6. J. Suntivich, H. A. Gasteiger, N. Yabuuchi, H. Nakanishi, J. B. Goodenough and Y. Shao-Horn, *Nat Chem*, 2011, 3, 546-550.
7. R. D. Smith, M. S. Prevot, R. D. Fagan, Z. Zhang, P. A. Sedach, M. K. Siu, S. Trudel and C. P. Berlinguette, *Science*, 2013, 340, 60-63.
8. M. W. Kanan and D. G. Nocera, *Science*, 2008, 321, 1072-1075.
9. K. Zeng and D. Zhang, *Progress in Energy and Combustion Science*, 2010, 36, 307-326.
10. A. Marshall, B. Børresen, G. Hagen, M. Tsytkin and R. Tunold, *Energy*, 2007, 32, 431-436.
11. E. Zoulias, E. Varkaraki, N. Lymberopoulos, C. N. Christodoulou and G. N. Karagiorgis, "A Review on Water Electrolysis", *TCJST*, 2004, 4(2), 41-71.
12. V. M. Nikolic, G. S. Tasic, A. D. Maksic, D. P. Saponjic, S. M. Miulovic and M. P. Marceta Kaninski, *International Journal of Hydrogen Energy*, 2010, 35, 12369-12373.
13. S. Marini, P. Salvi, P. Nelli, R. Pesenti, M. Villa, M. Berrettoni, G. Zangari and Y. Kiros, *Electrochimica Acta*, 2012, 82, 384-391.

14. A. Manabe, M. Kashiwase, T. Hashimoto, T. Hayashida, A. Kato, K. Hirao, I. Shimomura and I. Nagashima, *Electrochimica Acta*, 2013, 100, 249-256.
15. M. Bodner, A. Hofer and V. Hacker, *Wiley Interdisciplinary Reviews: Energy and Environment*, 2014.
16. M. Carmo, D. L. Fritz, J. Mergel and D. Stolten, *International Journal of Hydrogen Energy*, 2013, 38, 4901-4934.
17. J. R. Varcoe, M. Beillard, D. M. Halepoto, J. P. Kizewski, S. Poynton and R. C. T. Slade, *ECS Transactions*, 2008, **16**, 1819-1834.
18. Y. Leng, G. Chen, A. J. Mendoza, T. B. Tighe, M. A. Hickner and C. Y. Wang, *J Am Chem Soc*, 2012, 134, 9054-9057.
19. J. R. Varcoe, P. Atanassov, D. R. Dekel, A. M. Herring, M. A. Hickner, P. A. Kohl, A. R. Kucernak, W. E. Mustain, K. Nijmeijer, K. Scott, T. Xu and L. Zhuang, *Energy Environ. Sci.*, 2014, 7, 3135-3191.
20. M. K. Datta, K. Kadakia, O. I. Velikokhatnyi, P. H. Jampani, S. J. Chung, J. A. Poston, A. Manivannan and P. N. Kumta, *Journal of Materials Chemistry A*, 2013, 1, 4026.
21. R. Subbaraman, N. Danilovic, P. P. Lopes, D. Tripkovic, D. Strmcnik, V. R. Stamenkovic and N. M. Markovic, *The Journal of Physical Chemistry C*, 2012, 116, 22231-22237.
22. T. Reier, M. Oezaslan and P. Strasser, *ACS Catalysis*, 2012, 2, 1765-1772.
23. Y.-H. Fang and Z.-P. Liu, *Journal of the American Chemical Society*, 2010, **132**, 18214-18222.
24. Y. Lee, J. Suntivich, K. J. May, E. E. Perry and Y. Shao-Horn, *The Journal of Physical Chemistry Letters*, 2012, 399-404.

25. R. L. Doyle, I. J. Godwin, M. P. Brandon and M. E. Lyons, *Physical chemistry chemical physics: PCCP*, 2013, 15, 13737-13783.
26. R. Subbaraman, D. Tripkovic, K. C. Chang, D. Strmcnik, A. P. Paulikas, P. Hirunsit, M. Chan, J. Greeley, V. Stamenkovic and N. M. Markovic, *Nature materials*, 2012, 11, 550-557.
27. Y. Liang, Y. Li, H. Wang, J. Zhou, J. Wang, T. Regier and H. Dai, *Nature materials*, 2011, 10, 780-786.
28. M. R. Gao, Y. F. Xu, J. Jiang, Y. R. Zheng and S. H. Yu, *J Am Chem Soc*, 2012, 134, 2930-2933.
29. D. U. Lee, B. J. Kim and Z. Chen, *Journal of Materials Chemistry A*, 2013, 1, 4754.
30. D. Chanda, J. Hnát, M. Paidar and K. Bouzek, *International Journal of Hydrogen Energy*, 2014, 39, 5713-5722.
31. J. P. Singh and R.N.Singh, *J. New Mat. Electrochem. Systems*, 2000, 3, 131-139.
32. F. Cheng, J. Shen, B. Peng, Y. Pan, Z. Tao and J. Chen, *Nat Chem*, 2011, 3, 79-84.
33. M. Raghasudha, D. Ravinder and P. Veerasomaiah, *Advances in Materials Physics and Chemistry*, 2013, 03, 89-96.
34. S. Ida, K. Yamada, T. Matsunaga, H. Hagiwara, Y. Matsumoto and T. Ishihara, *Journal of the American Chemical Society*, 2010, 132, 17343-17345.
35. E. Mirzakułova, R. Khatmullin, J. Walpita, T. Corrigan, N. M. Vargas-Barbosa, S. Vyas, S. Oottikkal, S. T. Takeguchi, T. Yamanaka, H. Takahashi, H. Watanabe, T. Kuroki, H. Nakanishi, Y. Oriķasa, Y. Uchimoto, H. Takano, N. Ohguri, M. Matsuda, T. Murota, K. Uosaki and W. Ueda, *Journal of the American Chemical Society*, 2013, 135, 11125-11130.

36. T. Takeguchi, T. Yamanaka, H. Takahashi, H. Watanabe, T. Kuroki, H. Nakanishi, Y. Orikasa, Y. Uchimoto, H. Takano, N. Ohguri, M. Matsuda, T. Murota, K. Uosaki and W. Ueda, *Journal of the American Chemical Society*, 2013, **135**, 11125-11130.
37. D. E. Hall, *Journal of The Electrochemical Society*, 1985, **132**, 41C-48C.
38. F. Manzer, C. M. Hadad and K. D. Glusac, *Nat Chem*, 2012, **4**, 794-801.
39. X. Wu and K. Scott, *Journal of Materials Chemistry*, 2011, **21**, 12344.
40. X. Wu and K. Scott, *International Journal of Hydrogen Energy*, 2013, **38**, 3123-3129.
41. L. Xiao, S. Zhang, J. Pan, C. Yang, M. He, L. Zhuang and J. Lu, *Energy & Environmental Science*, 2012, **5**, 7869.
42. N. K. Singh, S. K. Tiwari, K. L. Anitha and R. N. Singh, *Journal of the Chemical Society, Faraday Transactions*, 1996, **92**, 2397.
43. Y. Fu, P. Xiong, H. Chen, X. Sun and X. Wang, *Industrial & Engineering Chemistry Research*, 2012, **51**, 725-731.
44. C. Iwakura, M. Nishioka and H. Tamura, *Nippon Kagaku Kaishi*, 1982, **7**, 136.
45. H. Zhu, S. Zhang, Y. X. Huang, L. Wu and S. Sun, *Nano letters*, 2013, **13**, 2947-2951.
46. T. Pandiarajan, S. Ravichandran and L. J. Berchmans, *RSC Adv.*, 2014, **4**, 64364-64370.
47. L. J. Berchmans, M. P. I. Devi and K. Amalajyothi, *International Journal of Self-Propagating High-Temperature Synthesis*, 2009, **18**, 11-14.
48. Y. Gorlin, B. Lassalle-Kaiser, J. D. Benck, S. Gul, S. M. Webb, V. K. Yachandra, J. Yano and T. F. Jaramillo, *Journal of the American Chemical Society*, 2013, **135**, 8525-8534.
49. M. Gong, Y. Li, H. Wang, Y. Liang, J. Z. Wu, J. Zhou, J. Wang, T. Regier, F. Wei and H. Dai, *Journal of the American Chemical Society*, 2013, **135**, 8452-8455.

50. L. Zhang and Y. Wu, *J. Nanomater.*, 2013, 2013, 1–6.
51. A. Mukherjee, S. Basu, P. K. Manna, S. M. Yusuf and M. Pal, *Journal of Materials Chemistry C*, 2014, 2, 5885-5891.
52. M. Jean-Baptiste, *Journal of Physics D: Applied Physics*, 2013, 46, 143001.
53. J. Hou, W. Jiang, Y. Fang and F. Huang, *J. Mater. Chem. C*, 2013, 1, 5892.
54. D. Channei, B. Inceesungvorn, N. Wetchakun, S. Ukritnukun, A. Nattestad, J. Chen and S. Phanichphant, *Sci. Rep.*, 2014, 4.
55. Y. Fukuda, S. Nagata and K. Echizenya, *Journal of Magnetism and Magnetic Materials*, 2004, 279, 325-330.
56. A. Tawfik, Y. Atassi, and I. S. Daewish, *Latv. J. Phys. Tech. Sci.*, 2005, N3, 68–74.
57. B. Parvatheeswara Rao and K. H. RAO *Journal of Materials Science*, 1997, **32**, 6049 – 6054.
58. D.W.stefan, *Coord Chem Rev*, 1989, **95**, **41**.
59. M. Mamlouk and K. Scott, *Journal of Power Sources*, 2012, 211, 140-146.
60. Y. Zhang, C. Wang, N. Wan, Z. Liu and Z. Mao, *Electrochemistry Communications*, 2007, 9, 667-670.
61. H. Ito, T. Maeda, A. Nakano, A. Kato and T. Yoshida, *Electrochimica Acta*, 2013, 100, 242-248.

Figure captions:

1. XRD patterns of $\text{Ce}_x\text{MnFe}_{2-x}\text{O}_4$ with $X=0.0, 0.2, 0.4, 0.6, 0.8$

2. (A).XPS spectra of the $\text{Ce}_{0.2}\text{MnFe}_{1.8}\text{O}_4$ after sintering
(B).EDAX spectra of $\text{Ce}_{0.2}\text{MnFe}_{1.8}\text{O}_4$ after sintering
3. XPS spectra of the catalysts. Insert XPS spectra of (a) Mn^{2+} (b) Ce^{3+} (c) Fe^{2+} & Fe^{3+} on as prepared $\text{Ce}_{0.2}\text{MnFe}_{1.8}\text{O}_4$ and (d) Fe^{2+} & Fe^{3+} on $\text{Ce}_{0.2}\text{MnFe}_{1.8}\text{O}_4$ after sintering.
4. SEM images of $\text{Ce}_x\text{MnFe}_{2-x}\text{O}_4$ ($X=0.0, 0.2$). Insert (A &B) before sintering and (C & D) after sintering.
5. Cyclic voltammograms of $\text{Pt}/\text{Ce}_x\text{MnFe}_{2-x}\text{O}_4$ ($X=0.0\leq 0.8$) at 25°C , with scan rate 10 mV/s in 1M KOH solution
6. Electrochemical impedance spectra of catalysts as a function of Ce substitution, measured at 1.6V during oxygen evolution
7. Schematic diagram of the single cell.
8. Polarisation curves of the MEA with $\text{Ce}_{0.2}\text{MnFe}_{1.8}\text{O}_4$, MnFe_2O_4 and without catalysts in deionised water at 25°C .
9. Nyquist plots for MEA with $\text{Ce}_{0.2}\text{MnFe}_{1.8}\text{O}_4$ as a function of potential from 1.50 to 1.75V during oxygen evolution reaction.
10. Tafel plots of OER current in fig. (8)
11. Chronopotentiometry curve of single with $\text{Ce}_{0.2}\text{MnFe}_{1.8}\text{O}_4$ under current density of $200\text{mA}/\text{cm}^2$.
12. Current density profile for constant electrolysis of MEA using MnFe_2O_4 and $\text{Ce}_{0.2}\text{MnFe}_{1.8}\text{O}_4$ with deionised water at applied potential of 2V at 25°C

Table captions:

1. OER activity of various anode materials recorded in deionized water.
2. Electrode Kinetic parameters for OER in deionized water.

Figure:

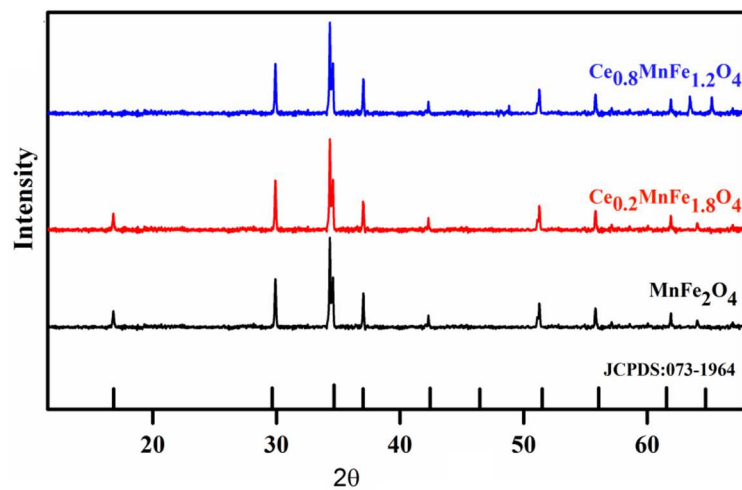


Figure:1

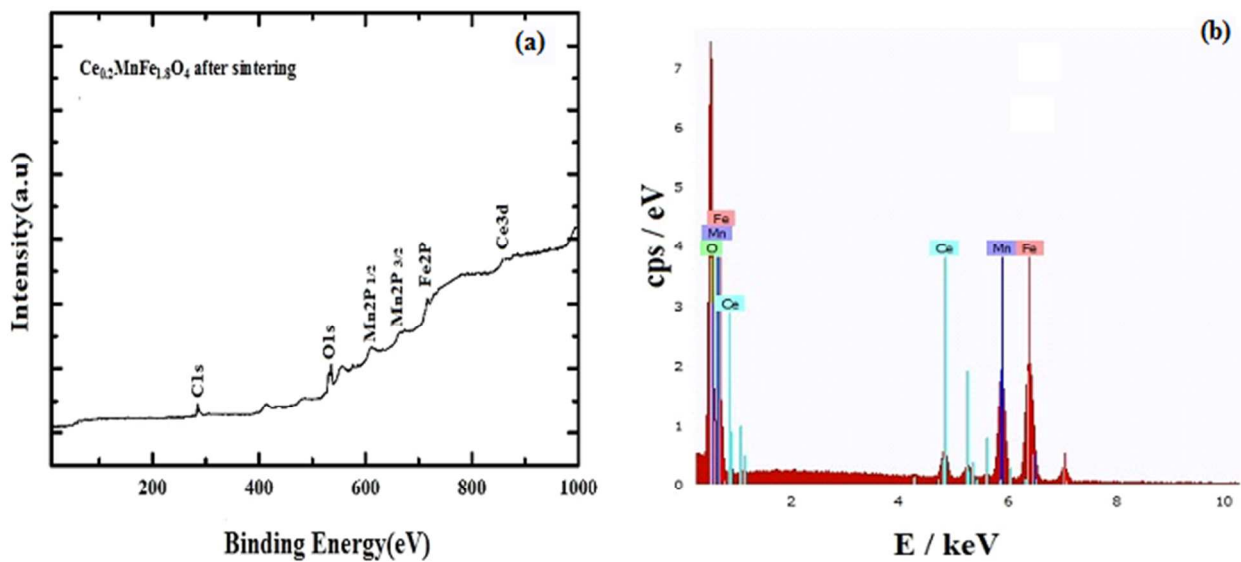


Figure: 2

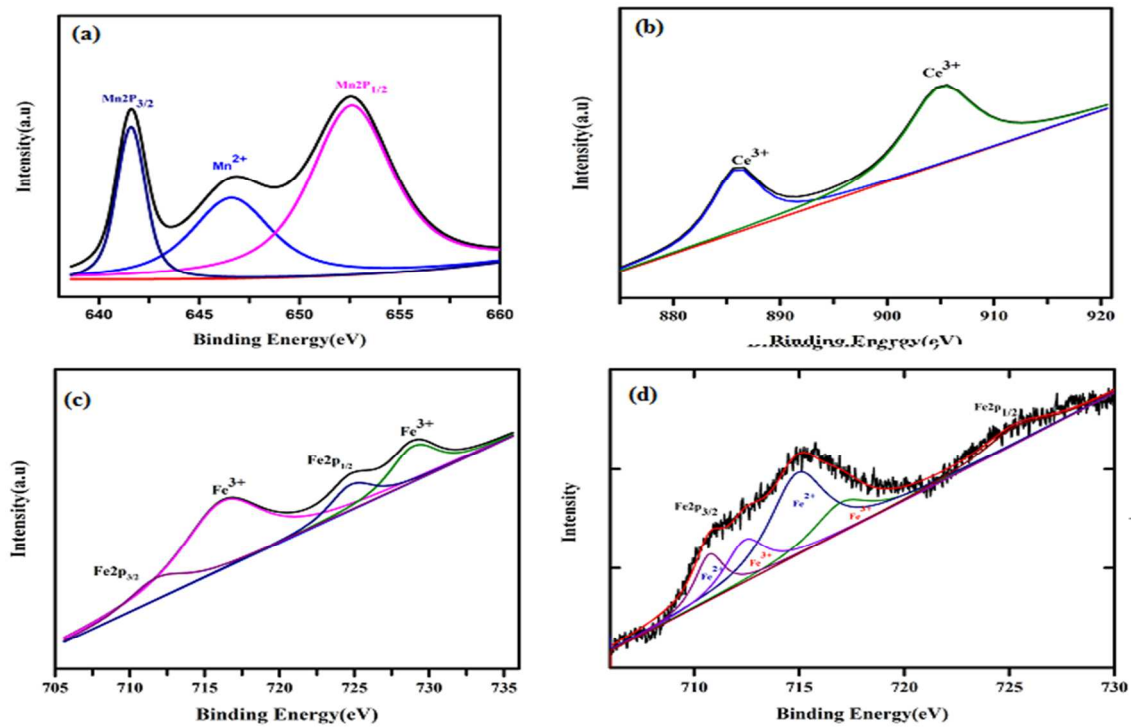


Figure: 3

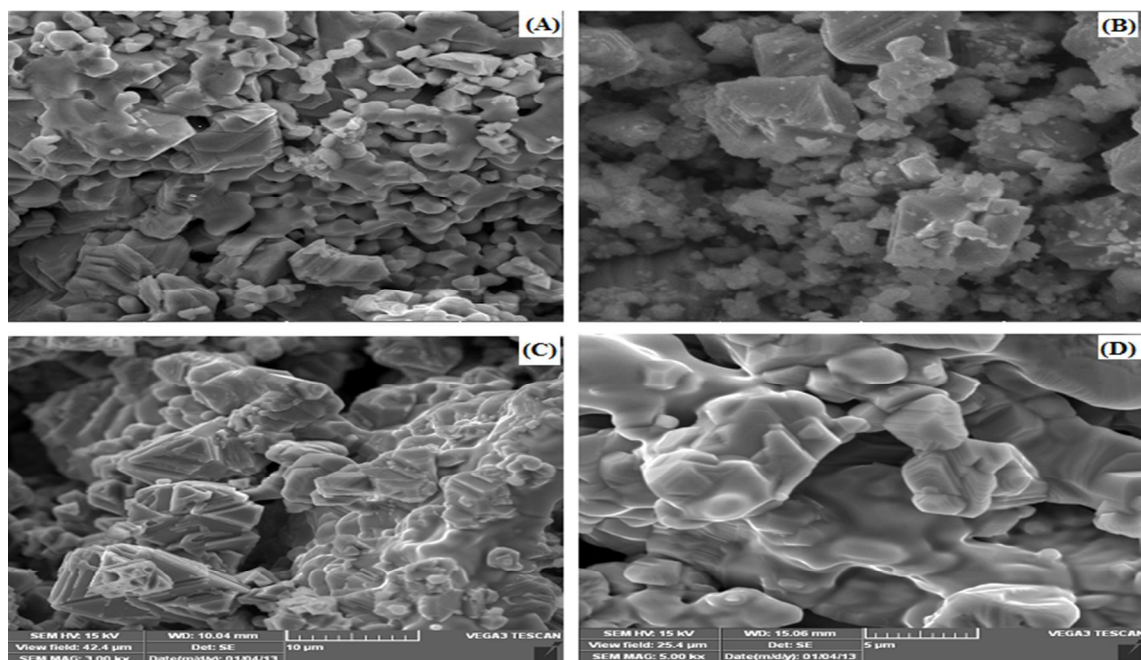


Figure: 4

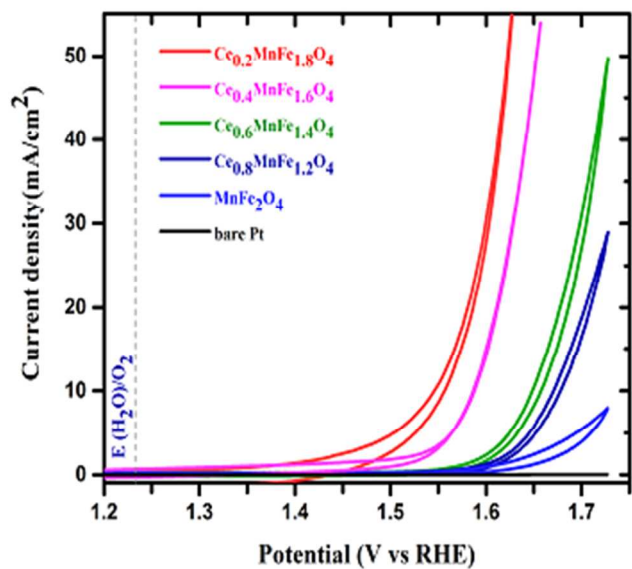


Figure: 5

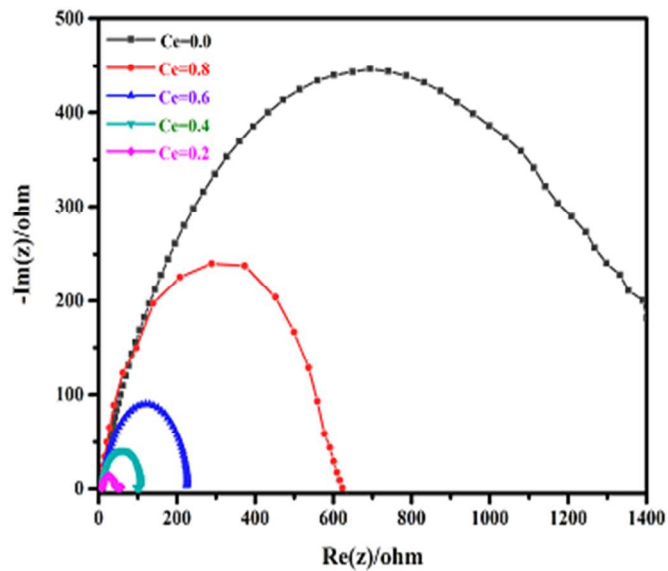


Figure: 6

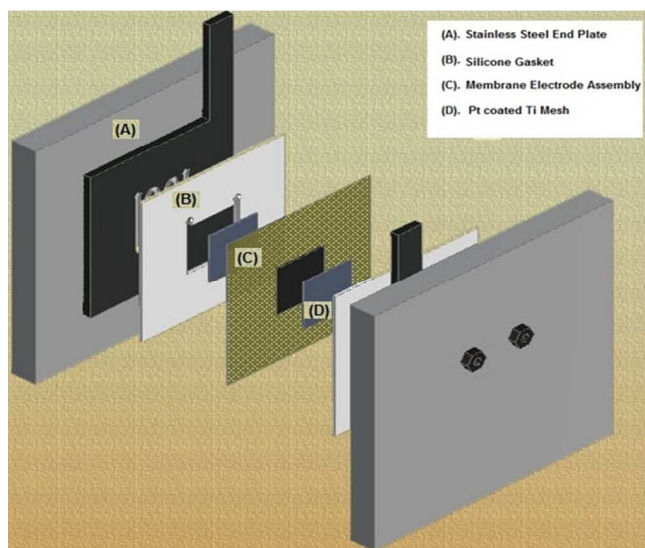


Figure :7

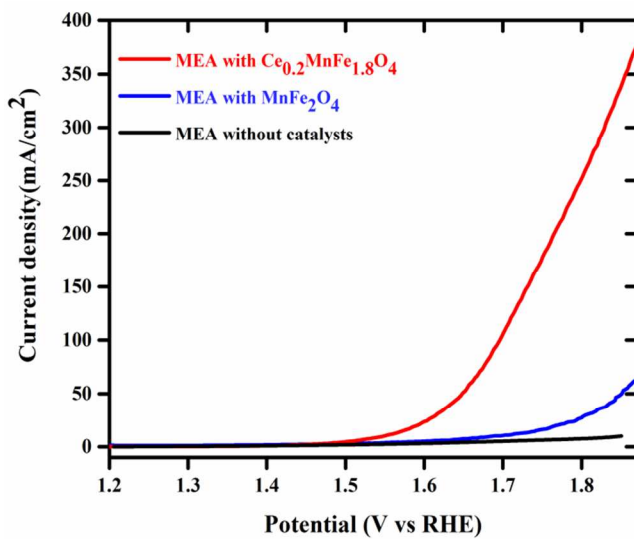


Figure:8

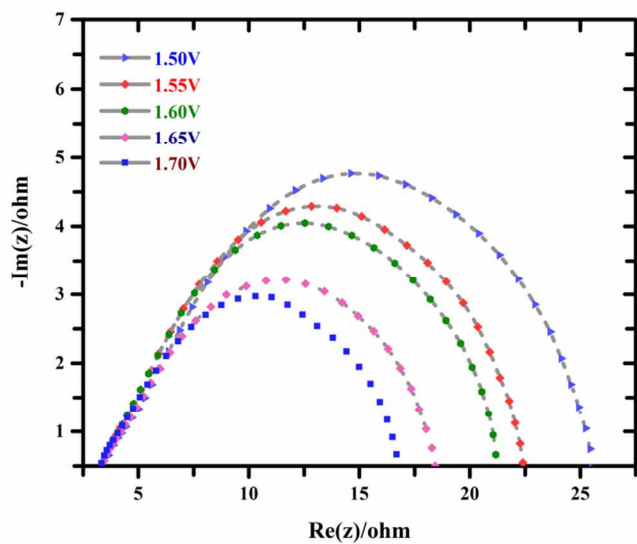


Figure:9

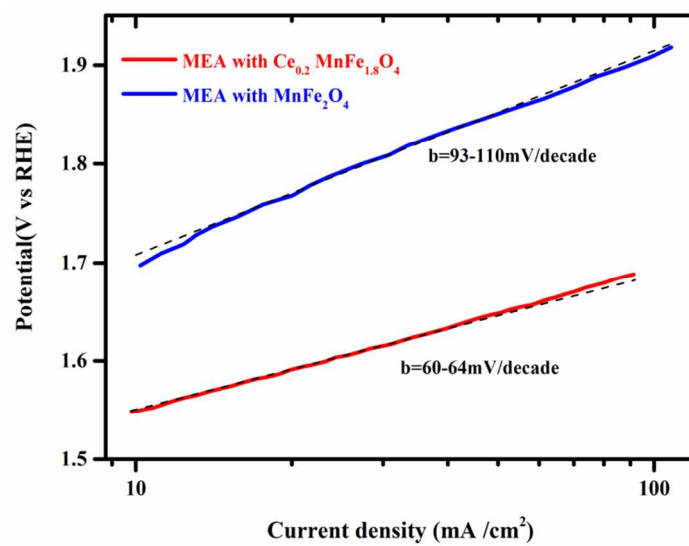


Figure:10

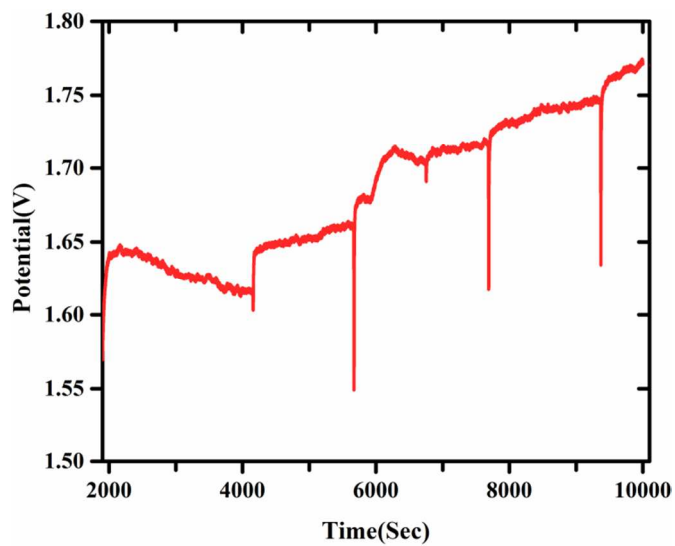


Figure:11

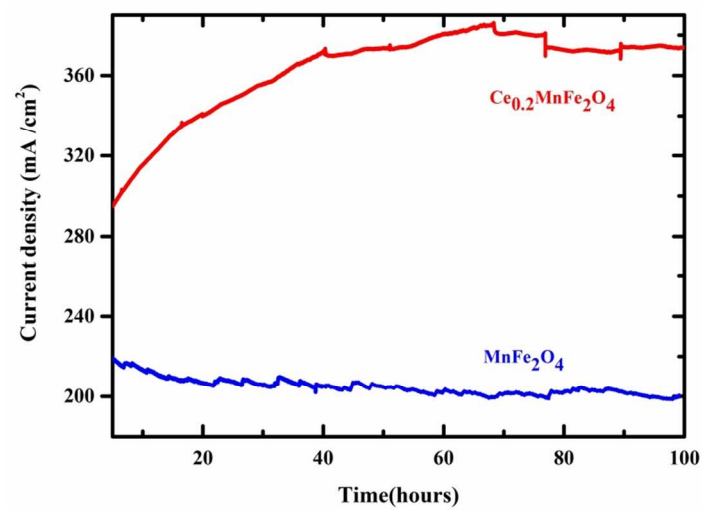


Figure:12

Table:

S.No	Anode Material	Operating Potential (V)	Temperature (°C)	Current Density (mA/cm ²)	Reference
(1).	Ce _{0.2} MnFe _{1.8} O ₄	1.8	25	300	This work
(2).	Li _{0.21} Co _{2.79} O ₄	2.2-2.05	20-45	300	Ref.39
(3).	IrO ₂	1.8	50	399	Ref.17
(4).	Cu _{0.7} Co _{2.3} O ₄	2.0	25	200	Ref.38
(5).	Ni-Fe	1.85	70	400	Ref.40

Table: 1

S. No	Catalysts	Lattice parameter (Å)	η_{O_2} (mV) at current density(j)			Tafel slope value(b) mV/decade
			10mA/cm ²	100mA/cm ²	300mA/cm ²	
1	Ce _{0.2} MnFe _{1.8} O ₄	8.614	320	460	570	64
2	MnFe ₂ O ₄	8.515	390	690	910	95

Table: 2